COMPARISON OF SLIDING-SURFACE AND MOVING-BAND TECHNIQUES IN FREQUENCY-DOMAIN FINITE-ELEMENT MODELS OF ROTATING MACHINES

Herbert De Gersem[1], Johan Gyselinck[2], Patrick Dular[2], Kay Hameyer[3], Thomas Weiland[1]

[1]**Technische Universität Darmstadt, Computational Electromagnetics Laboratory (TEMF)**
Schlossgartenstraße 8, D–64289 Darmstadt, Germany
[2]**University of Liège, Belgium, Dept. of Electrical Engineering (ELAP), Institut Montefiore**
Sart Tilman – B.28, B–4000 Liège, Belgium
[3]**Katholieke Universiteit Leuven, Belgium, Dep. ESAT, Div. ELECTA**
Kasteelpark Arenberg 10, B–3001 Leuven-Heverlee, Belgium
email: DeGersem/Weiland@temf.de; Johan.Gyselinck/Patrick.Dular@ulg.ac.be;
Kay.Hameyer@esat.kuleuven.ac.be

ABSTRACT

The sliding-surface and moving-band techniques are introduced in frequency-domain finite element formulations to model the solid-body motion of the rotors in an cylindrical machine. Both techniques are compared concerning their feasibility and computational efficiency. A frequency-domain model of a capacitor motor is equipped with a sliding surface and compared to a transient model with moving band. This example illustrates the advantages of frequency-domain simulation over transient simulation for the simulation of steady-state working conditions of electrical machines.

I. INTRODUCTION

One of the most important design criteria for electrotechnical devices is given by their characteristics for steady-state operation. Properties such as e.g. efficiency, produced torque, magnitude of the effective current, harmonic contents of currents and voltages, temperature rise at nominal operation are examined prior to fine tuning the design towards characteristics of secondary importance. The nominal operation mode of almost all electrical energy transducers is an operation at steady-state, i.e. periodically changing currents, voltages, speed and torque. For the numerical simulation of such conditions, frequency-domain formulations may be advantageous over transient formulations, especially when only a small number of a-priori known significant time-harmonic components are expected. Standard static and time-harmonic approaches are commonly applied to particular transformer and motor models. Neglecting the influence of higher harmonics, introduced by e.g. ferromagnetic saturation, non-linear loads, power electronic equipment and moving parts, is, however, only acceptable in specific cases. The increasing machine performance and the application of inverters necessitates to account for higher harmonic effects in the simulations. A multi-harmonic approach meets this requirement by considering a set of harmonic component at predefined frequencies [1]. The higher harmonics introduced by saturation and switching devices can be taken into account as illustrated by transformer examples. The application of the frequency-domain approach to models with moving parts, e.g. electrical machines, is not straightforward [2, 3]. The Lagrangian approach which is commonly applied for transient, motional eddy current simulation, ties different coordinate systems to each of the solid, moving or non-moving bodies. The continuity of the magnetic field is enforced by e.g. a moving-band approach [4] or a sliding-surface technique [5]. Although these techniques are well-established in transient simulation schemes, their application in frequency-domain formulations still causes numerical inconveniences. In this paper, the moving-band and sliding-surface techniques are introduced in frequency-domain FE models and compared for their efficiency.

II. MULTI-HARMONIC SIMULATION

A comparison is set up for a 2D frequency-domain finite-element (FE) model of a rotating machine, using the magnetodynamic formulation

$$-\frac{\partial}{\partial x}\left(\nu\frac{\partial A_z}{\partial x}\right)-\frac{\partial}{\partial y}\left(\nu\frac{\partial A_z}{\partial y}\right)+\sigma\frac{\partial A_z}{\partial t}=J_s \qquad (1)$$

in terms of the z-component A_z of the magnetic vector potential with ν the reluctivity, σ the conductivity and J_s the source current density. The coordinate system at the stator is denoted by (x, y) or in polar coordinates (r, θ). The coordinate systems at the rotor, i.e., (x', y') and (r, θ'), are related to those at the stator by $\theta' = \theta - \omega_m t$ with ω_m the constant angular mechanical velocity.

The frequency-domain finite-element (FE) technique applies a twofold weighted residual approach together with a twofold discretisation, i.e. a spatial discretisation of a domain Ω by a linear independent set of $n_{\rm fe}$ FE shape functions $\alpha_j(x, y)$ and a time discretisation at a temporal domain Υ over the time period T by an orthonormal set of $n_{\rm hm}$ harmonic functions $H_q(t)$ [6]. The harmonic functions are chosen from the set $\{1, \sqrt{2}\cos(\omega_q t), -\sqrt{2}\sin(\omega_q t)\}$ where 1 represents the DC components and ω_q belongs to a set of a-priori chosen electrical pulsations which are multiples of the fundamental pulsation $\omega_{\rm fund} = 2\pi/T$. The combined shape functions $\alpha_j(x, y)H_q(t)$ are basis functions for the product space combining both approximation spaces. The discretisation of the magnetic vector potential reads

$$A_z(x, y, t) = \sum_{j=1}^{n_{\rm fe}}\sum_{q=1}^{n_{\rm hm}} u_{j,q}\alpha_j(x, y)H_q(t)\ . \qquad (2)$$

The application of the Ritz-Galerkin technique, i.e. the weighing of the partial differential equation (1) with A_z dis-

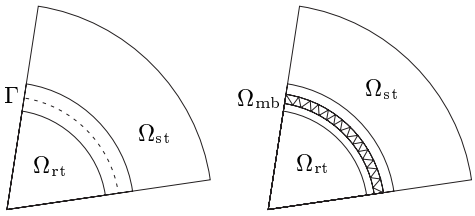

Fig. 1: (a) Sliding-surface and (b) moving-band techniques for an electrical machine model.

cretised by (2) results in the system of equations

$$\mathbf{K}\mathbf{u} = \mathbf{f} \tag{3}$$

where

$$\begin{aligned}\mathbf{K}_{i,p,j,q} &= \int_\Omega \int_\Upsilon \left(\nu H_p H_q \nabla\alpha_i \cdot \nabla\alpha_j \right. \\ &+ \left. \sigma H_p \frac{dH_q}{dt}\alpha_i\alpha_j\right) \mathrm{d}t\,\mathrm{d}x\mathrm{d}y \ ; \qquad (4)\\ \mathbf{f}_{i,p} &= \int_\Omega \int_\Upsilon J_s \alpha_i H_q \,\mathrm{d}t\,\mathrm{d}x\mathrm{d}y \ . \qquad (5)\end{aligned}$$

The particular choice of harmonic functions H_q as the temporal shape functions characterises the frequency-domain approach. Due to the fact that temporal shape functions are orthonormal in Υ, the system matrix $\mathbf{K}$ has a block diagonal structure when the equations are ordered according to the spatial shape functions first.

III. MACHINE MODEL

The stator and rotor domains Ω_{st} and Ω_{rt} are treated independently. Different sets of temporal harmonics are allowed for both domains. The frequency-domain FE discretisation reads

$$\begin{aligned}\mathbf{K}_{\mathrm{st}}\mathbf{u}_{\mathrm{st}} &= \mathbf{f}_{\mathrm{st}} \ ; \qquad (6)\\ \mathbf{K}_{\mathrm{rt}}\mathbf{u}_{\mathrm{rt}} &= \mathbf{f}_{\mathrm{rt}} \ . \qquad (7)\end{aligned}$$

When a *sliding-surface* technique is applied, the stator domain Ω_{st} and the rotor domain Ω_{rt} share the common circular interface $\Gamma = \Omega_{\mathrm{st}} \cap \Omega_{\mathrm{rt}}$ in the air gap of the rotating device (Fig. 1). When constructing (6) and (7), independent degrees of freedom are considered at the stator and rotor sides of Γ. In case of the *moving-band* approach, a single layer of finite elements is constructed in a small circular domain Ω_{mb}, situated in the air gap of the machine between Ω_{st} and Ω_{rt} [4]. The connection between the inner boundary of the stator and the outer boundary of the rotor is discussed in the following sections.

The distribution of the magnetic vector potential at a circle in the air gap can be decomposed in a sum of rotating waves

$$u(\theta,t) = \sum_p \sum_k u_{p,k} \cos\left(\omega_p t - \lambda_k \theta - \phi_{p,k}\right) \tag{8}$$

where ω_p, λ_k and $\phi_{p,k}$ denote the pulsation, the pole-pair number and the phase of the wave and $u_{p,k}$ are unknown coefficients. An observer attached to the rotor experiences the air-gap field

$$u'(\theta',t) = \sum_p \sum_k u_{p,k} \cos\left(\tilde{\omega}_{p,k} t - \lambda_k \theta' - \phi_{p,k}\right) \ , \tag{9}$$

i.e., a linear combination of waves with the same pole-pair numbers and phases, but at the *slip* pulsations $\tilde{\omega}_{p,k} = \omega_p - \lambda_k \omega_m$. Hence, the selection of the set of harmonics to be considered at the rotor, not only depends on the harmonics present in the stator but also on the spatial-harmonic contents expected for the air-gap field, e.g. the higher harmonics introduced by the winding scheme and those due to the slotting of stator and rotor.

IV. SLIDING-SURFACE TECHNIQUE

Several sliding-surface techniques can be distinguished based on the choice of method for enforcing the continuity at the common interface. In general, the stator and rotor meshes at Γ do not match for all positions attained during the time integration. Hence, the field at one of both sides has to be interpolated [7] or mortar-projected [5] on the mesh of the other side. A third non-matching mesh treatment which is particularly efficient for rotating devices, is a mortar-element method with harmonic test functions as proposed in [8]. This approach is particularly suited in case of a frequency-domain FE formulation and is favoured here.

The continuity of the magnetic vector potential at the sliding surface is enforced by weighing the difference between the magnetic vector potential at Γ with the spatial harmonic test functions $\xi_{k,p}(\theta,t) = G_k(\theta)H_p(t)$ where $G_k(\theta) \in \{1, \sqrt{2}\cos(\lambda_k\theta), -\sqrt{2}sin(\lambda_k\theta)\}$ and $\lambda_k \in \mathbb{N}$. The resulting constraint equation is

$$\mathbf{B}_{\mathrm{st}}\mathbf{u}_{\mathrm{st}} - \mathbf{B}_{\mathrm{rt}}\mathbf{u}_{\mathrm{rt}} = 0 \tag{10}$$

where

$$\begin{aligned}\mathbf{B}_{\mathrm{st},k,p,j,q} &= \int_\Gamma \int_\Upsilon \alpha_j(\theta) H_q(t) G_k(\theta) H_p(t) \,\mathrm{d}\theta\,\mathrm{d}t \ ; \\ \mathbf{B}_{\mathrm{rt},k,p,j,q} &= \int_\Gamma \int_\Upsilon \alpha_j(\theta') H_q(t) \\ &\quad G_k(\theta' + \omega_m t) H_p(t) \,\mathrm{d}\theta\,\mathrm{d}t \ . \qquad (11)\end{aligned}$$

The constraints are added to the formulation using a set of Lagrange multipliers $\mathbf{z}$, resulting in the saddle-point model

$$\begin{bmatrix} \mathbf{K}_{\mathrm{st}} & 0 & \mathbf{B}_{\mathrm{st}}^H \\ 0 & \mathbf{K}_{\mathrm{rt}} & -\mathbf{B}_{\mathrm{rt}}^H \\ \mathbf{B}_{\mathrm{st}} & -\mathbf{B}_{\mathrm{rt}} & 0 \end{bmatrix} \begin{bmatrix} \mathbf{u}_{\mathrm{st}} \\ \mathbf{u}_{\mathrm{rt}} \\ \mathbf{z} \end{bmatrix} = \begin{bmatrix} \mathbf{f}_{\mathrm{st}} \\ \mathbf{f}_{\mathrm{rt}} \\ 0 \end{bmatrix} \ . \tag{12}$$

If a sliding surface is applied at a circular interface with an equidistant grid, the computational cost of the operators $\mathbf{B}_{\mathrm{st}}$ and $\mathbf{B}_{\mathrm{rt}}$ can be reduced considerably by weighing the magnetic vector potential at a discrete set of points, e.g. at the FE vertices at Γ [9]. Then, the discretisation is no longer conforming, but the integrations in (11) can be rearranged such that the Fast Fourier Transform (FFT) $\mathbf{F}$ instead of the dense matrices $\mathbf{B}_{\mathrm{st}}$ and $\mathbf{B}_{\mathrm{rt}}$, for each temporal harmonic separately:

$$\begin{aligned}\mathbf{B}_{\mathrm{st},p,q} &= \delta_{pq}\mathbf{F} \qquad (13)\\ \mathbf{B}_{\mathrm{rt},p,q} &= \mathbf{R}_{pq}\mathbf{F} \qquad (14)\end{aligned}$$

where $\mathbf{R}_{k,p,k,q} = 1$ if $\omega_p = \omega_q - \lambda_k\omega_m$, i.e. if the pulsation ω_p at the rotor side matches the slip pulsation introduced by the air-gap wave with pulsation ω_q and pole pair number λ_k. The approach with the FFT does not account for the curvature of Γ and the exact distribution of the magnetic vector

Table 1: Asymptotic order of the computational complexity of the individual system matrix components.

matrix	$\mathbf{K}_{\mathrm{st}}$	$\mathbf{K}_{\mathrm{mb}}$	$\mathbf{B}_{\mathrm{st}}$	$\mathbf{B}_{\mathrm{st}}$ (FFT)
	$\mathbf{K}_{\mathrm{rt}}$		$\mathbf{B}_{\mathrm{rt}}$	$\mathbf{B}_{\mathrm{rt}}$ (FFT)
order	$n_{\mathrm{hm}} n_{\mathrm{fe}}$	$n_{\mathrm{hm}} n_{\mathrm{fe}}$	$n_{\mathrm{hm}} n_{\mathrm{fe}}$	$n_{\mathrm{hm}} \sqrt{n_{\mathrm{fe}}} \log \sqrt{n_{\mathrm{fe}}}$

potential between the FE vertices at Γ. This approximation is, however, acceptable for many machine models as long as a sufficient fine discretisation is constructed at Γ.

V. MOVING-BAND TECHNIQUE

A *moving-band* Ω_{mb} is a small circular domain situated in the air gap of the machine in which a single layer of finite elements is constructed [4] (Fig. 1). The moving band is remeshed for every angular position. Hence, the supports of the spatial FE shape functions in the moving band change depending on the position. The contributions of the elements of Ω_{mb} read, e.g. for $i \in \Omega_{\mathrm{st}}$ and $j \in \Omega_{\mathrm{rt}}$,

$$\mathbf{K}_{\mathrm{mb,st,rt},i,p,j,q} = \int_{\Omega_{\mathrm{mb}}} \int_{\Upsilon} \nu H_p(t) H_q(t) \nabla \alpha_i(x,y) \cdot \nabla \alpha_j(x',y') \,\mathrm{d}t \,\mathrm{d}x \,\mathrm{d}y \,. \quad (15)$$

Since the relation between the coordinate systems (x, y) and (x', y') and overlap of the supports of two spatial FE shape functions $\alpha_i(x, y)$ and $\alpha_j(x', y')$ depend on the velocity and the time, the contributions of elements of Ω_{mb} to the stiffness matrix result in a full coupling between all harmonics [10]. The combined system of equations is

$$\begin{bmatrix} \mathbf{K}_{\mathrm{st}} + \mathbf{K}_{\mathrm{mb,st,st}} & \mathbf{K}_{\mathrm{mb,st,rt}} \\ \mathbf{K}_{\mathrm{mb,rt,st}} & \mathbf{K}_{\mathrm{rt}} + \mathbf{K}_{\mathrm{mb,rt,rt}} \end{bmatrix} \begin{bmatrix} \mathbf{u}_{\mathrm{st}} \\ \mathbf{u}_{\mathrm{rt}} \end{bmatrix} = \begin{bmatrix} \mathbf{f}_{\mathrm{st}} \\ \mathbf{f}_{\mathrm{rt}} \end{bmatrix} . \quad (16)$$

VI. COMPARISON BETWEEN MOVING-BAND AND SLIDING-SURFACE APPROACHES

a. Computational complexity

In case of a multi-harmonic formulation, the stator-rotor coupling gives rise to additional dense matrix parts or to dense constraint equations, both when using the moving-band technique or the sliding-surface approach. This is the main drawback for multi-harmonic formulations compared to transient formulations. The number of FE vertices at Γ scales as $\sqrt{n_{\mathrm{fe}}}$. The computational complexities of the individual components of the system matrix components are gathered in Table 1. The dense matrix pats $\mathbf{K}_{\mathrm{mb}}$, $\mathbf{B}_{\mathrm{st}}$ and $\mathbf{B}_{\mathrm{rt}}$ have the same complexity as the multi-harmonic FE system matrices $\mathbf{K}_{\mathrm{st}}$ and $\mathbf{K}_{\mathrm{rt}}$ themselves and, hence, may lead to a substantial increase of the computational cost of the algorithm. When the FFT-variant of the sliding-surface technique is applied, the asymptotical complexity of $\mathbf{B}_{\mathrm{st}}$ and $\mathbf{B}_{\mathrm{rt}}$ remains below the one of $\mathbf{K}_{\mathrm{st}}$ and $\mathbf{K}_{\mathrm{rt}}$. Hence, the stator-rotor coupling does not kill the numerical efficiency of multi-harmonic simulation.

b. Applicability

The moving-band technique also applies to models with more sophisticated motion patterns. The sliding-surface technique with harmonic test functions is restricted to circular interfaces or to integer parts of them. An efficient implementation of the sliding-surface technique moreover requires an equidistant mesh at the interface in the air gap. The construction of generally applicable preconditioners for the systems augmented with sliding-surface constraints is cumbersome [11].

c. Discretisation error

The moving-band technique yields conforming, variational formulations, i.e. the FE meshes match in the air gap and a constrained FE test and trial space is used for the magnetic vector potential. For the sliding-surface technique with FFTs, the discretisation is not matching at Γ and a saddle-point system is attained. The additional discretisation error introduced at Γ is acceptable for the models considered here.

d. Non-propagated harmonic components

A wave component at pulsation ω_p and pole-pair number λ_k induced by the stator in the air gap, corresponds to a wave at pulsation $\omega_q = \omega_p - \lambda_k \omega_m$ and pole-pair number λ_k observed by the rotor. A *non-propagated* harmonic components arises when either the component at pulsation ω_p is not considered at the stator or the component at pulsation ω_q is not considered at the rotor. The question arises which boundary conditions are inherently applied for these components in the air gap. Here, an important difference between the sliding-surface and the moving-band techniques is observed. In case of the moving-band approach, a wave component which is considered at the stator but not at the rotor vanishes at the boundary between the rotor and the moving band. Similarly, a component introduced by the rotor vanishes at the boundary between the stator and the moving band. Hence, non-propagated components experience homogeneous Dirichlet conditions at one of the boundaries of the moving band. As a consequence, the moving-band technique as presented here is flux-conservative in the air gap. In case of the presented sliding-surface technique, a stator harmonic component which is is not propagated to the rotor, does not vanish at the stator side of Γ. The non-propagated components experience a homogeneous Neumann constraint at the stator and rotor sides of Γ. This results in a discontinuous magnetic flux at Γ, even if an exact integration as in (11) and (11) is applied. The application of homogeneous Dirichlet constraints to non-propagated flux components requires the addition of additional constraints of the form $\mathbf{S}_{\mathrm{st}} \mathbf{F} \mathbf{u}_{\mathrm{st}} = 0$ and $\mathbf{S}_{\mathrm{rt}} \mathbf{F} \mathbf{u}_{\mathrm{rt}} = 0$ where $\mathbf{S}_{\mathrm{st}}$ selects all components with wave numbers (ω_p, λ_k) for which the corresponding slip pulsations $\omega_q = \omega_p - \lambda_k \omega_m$ are not considered at Ω_{rt} and $\mathbf{S}_{\mathrm{rt}}$ selects all components with wave numbers (ω_q, λ_ℓ) for which the corresponding excitation pulsations $\omega_p = \omega_q + \lambda_\ell \omega_m$ are not considered at Ω_{st}.

VII. CAPACITOR MOTOR EXAMPLE

Both techniques are compared for a capacitor motor induction machine. The motor has a nominal power of 0.75 kW, a nominal speed of 2760 rpm, a voltage of 230 V, a nominal current of 5.2 A and a $\cos\phi$ of 0.96. The main winding of the motor is connected directly to a single-phase alternating current supply whereas the auxiliary winding is connected through a capacitor of 19.7 μF. The stator has 24 slots

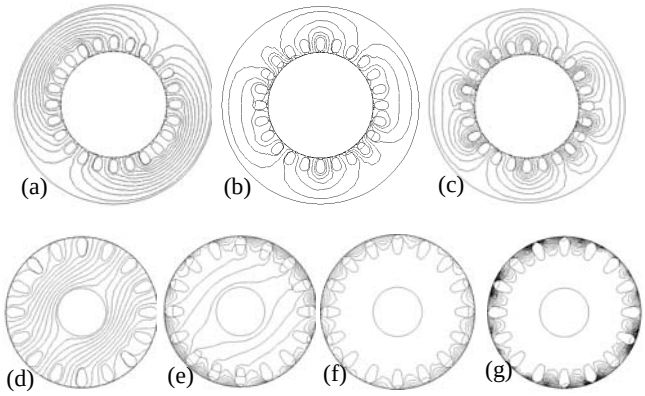

Fig. 2: Magnetic flux plot in the stator at (a) 50 Hz, (b) 750 Hz and (c) 850 Hz; magnetic flux plot in the rotor at (d) 0 Hz, (e) 100 Hz, (f) 800 Hz and (g) 900 Hz.

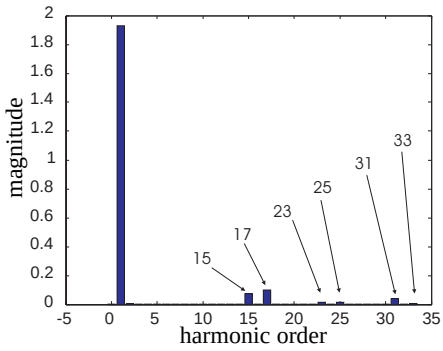

Fig. 3: Spectrum of the current through the main stator winding at no-load.

whereas the rotor has 16 slots. Here, as an example, the no-load behaviour of the capacitor motor is simulated. The power supply is assumed to be a perfect sine at 50 Hz. Due to ferromagnetic saturation, additional harmonic components are introduced at the stator of which only the 150 Hz and 250 Hz are considered in the frequency-domain approach. The air-gap field of a single-phase motor is elliptical. Hence, at no-load, there is besides the 0 Hz component, rotating synchronously to the forward rotating air-gap field, a significant component at 100 Hz introduced by the backward rotating air-gap field. Due to the slotting of the stator and rotor, substantial components at 750 Hz and 850 Hz are detected. The magnetic flux distributions for the different time-harmonic components are plotted in Fig. 2. The spectrum of the current through the main winding indicates that the slot harmonics at 750 and 850 Hz are substantially more important than the harmonics introduced by saturation (Fig. 3). A transient simulation of the start-up of the capacitor motor shows that a large number of periods have to be stepped through before reaching steady-state, which is not necessary when using a multi-harmonic approach as is proposed in this paper. For the capacitor motor model with 24832 FE nodes, the multi-harmonic simulation takes 16 min whereas the transient simulation requires 5 hours.

VIII. CONCLUSIONS

Multi-harmonic FE machine models require the solution of large systems of equations but may be advantageous over transient schemes which need to step through a start-up process before reaching steady-state.

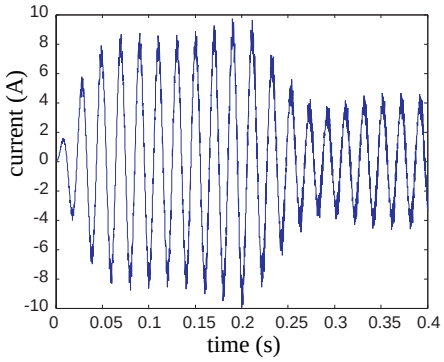

Fig. 4: Current through the main stator winding at start-up.

ACKNOWLEDGMENT

The research was carried out in the frame of the Inter-University Attraction Pole IAP P5/34 for fundamental research funded by the Belgian federal government. Herbert De Gersem is working in the cooperation project ”DA-WE1 (TEMF/GSI)” with the ”Gesellschaft für Schwerionenforschung (GSI)”, Darmstadt.

REFERENCES

[1] S. Yamada, K. Bessho, and J. Lu. Harmonic balance finite element method applied to nonlinear AC magnetic analysis. *IEEE Trans. Magn.*, 25(4):2971–2973, July 1989.

[2] G. Vinsard and B. Laporte. A new formulation for induction machine computation. *IEEE Trans. Magn.*, 30(5):3693–3696, September 1994.

[3] L. Vandevelde, J. Gyselinck, and J. Melkebeek. Steady-state finite element analysis in the frequency domain of inverter-fed squirrel cage induction motors. In *SPEEDAM*, pages 29–34, Taormina, Italy, June 1994.

[4] B. Davat, Z. Ren, and M. Lajoie-Mazenc. The movement in field modeling. *IEEE Trans. Magn.*, 21(6):2296–2298, November 1985.

[5] D. Rodger, H.C. Lai, and P.J. Leonard. Coupled elements for problems involving movement. *IEEE Trans. Magn.*, 26(2):548–550, March 1990.

[6] J. Gyselinck, P. Dular, C. Geuzaine, and W. Legros. Harmonic-balance finite-element modeling of electromagnetic devices: a novel approach. *IEEE Trans. Magn.*, 38(2):521–524, March 2002.

[7] R. Perrin-Bit and J.L. Coulomb. A three dimensional finite element mesh connection for problems involving movement. *IEEE Trans. Magn.*, 31(3), May 1995.

[8] H. De Gersem and T. Weiland. Harmonic weighting functions at the sliding interface of a finite element machine model incorporating angular displacement. In *COMPUMAG*, volume 1, pages 48–49, Saratoga Springs, New York, USA, July 2003.

[9] H. De Gersem and K. Hameyer. Air-gap flux splitting for the time-harmonic finite-element simulation of single-phase induction machines. *IEEE Trans. Magn.*, 38(2):1221–1224, March 2002.

[10] J. Gyselinck, L. Vandevelde, P. Dular, and C. Geuzaine. A general method for the frequency domain FE modeling of rotating electromagnetic devices. *IEEE Trans. Magn.*, 39(3):1147–1150, May 2003.

[11] H. De Gersem, S. Vandewalle, M. Clemens, and T. Weiland. Interface preconditioners for non-trivial interface conditions in air gaps of rotating electrical machines. 14th Int. Conf. Domain Decomposition Methods, Cocoyoc, Morelos, Mexico, January 2002.